Research Article | Vol. 25, No. 2 | 23 Jan 2017 | OPTICS EXPRESS 1073

Optics EXPRESS

Magnetic-field tuning of whispering gallery mode lasing from ferromagnetic nematic liquid crystal microdroplets

MARUŠA MUR,[1] JUNAID AHMAD SOFI,[2] IVAN KVASIĆ,[1] ALENKA MERTELJ,[1] DARJA LISJAK,[1] VIDUR NIRANJAN,[3] IGOR MUŠEVIČ,[1,4,5] AND SURAJIT DHARA[2,6]

[1]*Jozef Stefan Institute, Jamova cesta 39, 1000 Ljubljana, Slovenia*
[2]*School of Physics, University of Hyderabad, Hyderabad-500046, India*
[3]*National Institute of Technology Karnataka, Surathkal, Mangaluru-575025, India*
[4]*Faculty of Mathematics and Physics, University of Ljubljana, Jadranska ulica 19, 1000 Ljubljana, Slovenia*
[5]*igor.musevic@ijs.si*
[6]*sdsp@uohyd.ernet.in*

Abstract: We report magnetic field tuning of the structure and Whispering Gallery Mode lasing from ferromagnetic nematic liquid crystal micro-droplets. Microlasers were prepared by dispersing a nematic liquid crystal, containing magnetic nanoparticles and fluorescent dye, in a glycerol-lecithin matrix. The droplets exhibit radial director structure, which shows elastic distortion at a very low external magnetic field. The fluorescent dye doped ferromagnetic nematic droplets show Whispering Gallery Mode lasing, which is tunable by the external magnetic field. The tuning of the WGM lasing modes is linear in magnetic field with a wavelength-shift of the order of 1 nm/100 mT. Depending on the lasing geometry, the WGMs are red- or blue-shifted.

OCIS codes: (160.3710) Liquid crystals; (140.3945) Microcavities; (140.3600) Lasers, tunable; (280.3420) Laser sensors.

References and links

1. P. G. De Gennes and J. Prost, *The Physics of Liquid Crystals* (Oxford University, 1993).
2. H. Stark, "Physics of colloidal dispersions in nematic liquid crystals," Phys. Rep. **351**(6), 387–474 (2001).
3. I. Muševič, M. Škarabot, U. Tkalec, M. Ravnik, and S. Žumer, "Two-dimensional nematic colloidal crystals self-assembled by topological defects," Science **313**, 954–958 (2006).
4. A. Nych, U. Ognysta, M. Škarabot, M. Ravnik, S. Žumer, and I. Muševič, "Assembly and control of 3D nematic dipolar colloidal crystals," Nat. Commun. **4**, 1489 (2013).
5. I. I. Smalyukh, O. D. Lavrentovich, A. N. Kuzmin, A. V. Kachynski, and P. N. Prasad, "Elasticity-mediated self-organization and colloidal interactions of solid spheres with tangential anchoring in a nematic liquid crystal," Phys. Rev. Lett. **95**, 157801 (2005).
6. K. P. Zuhail, P. Sathyanarayana, D. Seč, S. Čopar, M. Škarabot, I. Muševič, and S. Dhara, "Topological defect transformation and structural transition of two-dimensional colloidal crystals across the nematic to smectic- A phase transition," Phys. Rev. E **91**, 030501(R) (2015).
7. K. P. Zuhail and S. Dhara, "Temperature dependence of equilibrium separation and lattice parameters of nematic boojum-colloids," Appl. Phys. Lett. **106**, 211901 (2015).
8. I. Muševič, "Liquid-crystal micro-photonics," Liquid Crystal Reviews **4**, 1–34 (2016).
9. A. Mertelj, D. Lisjak, M. Drofenik, and M. Čopič, "Ferromagnetism in suspensions of magnetic platelets in liquid crystal," Nature **504**, 237–241 (2013).
10. A. Mertelj, N. Osterman, D. Lisjak, and M. Čopič, "Magneto-optic and converse magnetoelectric effects in a ferromagnetic liquid crystal," Soft Matter **10**, 9065–9072 (2014).
11. R. Sahoo, M. V. Rasna, D. Lisjak, A. Mertelj, and S. Dhara, "Magnetodielectric and magnetoviscosity response of a ferromagnetic liquid crystal at low magnetic fields," Appl. Phys. Lett. **106**, 161905 (2015).
12. Q. Zhang, P. J. Ackerman, Q. Liu, and I. I. Smalyukh, "Ferromagnetic switching of knotted vector fields in liquid crystal colloids," Phys. Rev. Lett. **115**, 097802 (2015).
13. Q. Liu, P. J. Ackerman, T. C. Lubensky, and I. I. Smalyukh, "Biaxial ferromagnetic liquid crystal colloids," PNAS **113**(38), 10479–10484 (2016).

#279296 http://dx.doi.org/10.1364/OE.25.001073
Journal © 2017 Received 21 Oct 2016; revised 29 Dec 2016; accepted 2 Jan 2017; published 12 Jan 2017

Optics EXPRESS

14. M. Humar, M. Ravnik, S.Pajk, and I. Muševič, "Electrically tunable liquid crystal optical microresonators," Nat. Photonics **3**, 595–600 (2009).
15. M. Humar and I. Muševič, "3D microlasers from self-assembled cholesteric liquid-crystal microdroplets," Opt. Express **18**, 26995–27003 (2010).
16. D. J. Gardiner, S. M. Morris, P. J. W. Hands, C. Mowatt, R. Rutledge, T. D. Wilkinson, and H. J. Coles, "Paintable band-edge liquid crystal lasers," Opt. Express **19**, 2432–2439 (2011).
17. J.-D. Lin, M.-H. Hsieh, G.-J. Wei, T.-S. Mo, S.-Y. Huang, and C.-R. Lee, "Optically tunable/switchable omnidirectionally spherical microlaser based on a dye-doped cholesteric liquid crystal microdroplet with an azo-chiral dopant," Opt. Express **21**, 15765–15776 (2013).
18. Z. Zheng, B. Liu L. Zhou, W. Wang, W. Hu, and D. Shen, "Wide tunable lasing in photoresponsive chiral liquid crystal emulsion," J. Mater. Chem. C **3**, 2462–2470 (2015).
19. M. Humar and I. Muševič, "Surfactant sensing based on whispering-gallery-mode lasing in liquid-crystal microdroplets," Opt. Express **21**, 19836–19844 (2011).
20. M. Humar and I. Muševič, "Lasing and waveguiding in smectic A liquid crystal optical fibers," Opt. Express **21**, 19836–19844 (2011).
21. T. A. Kumar, M. A. Mohiddon, N. Dutta, N. K. Viswanathan, and S. Dhara, "Detection of phase transitions from the study of whispering gallery mode resonance in liquid crystal droplets," Appl. Phys. Lett. **106**, 051101 (2015).
22. A. Mahmood, V. Kavungal, S. S. Ahmed, G. Farrell, and Y. Semenova"Magnetic-field sensor based on whispering-gallery modes in a photonic crystal fiber infiltrated with magnetic fluid," Opt. Lett. **40**(21), 4983–4986 (2015).
23. D. Lisjak, and M. Drofenik, "Chemical substitution - an alternative strategy for controlling the particle size of barium ferrite," Cryst. Growth Des. **12**(11), 5174–5179 (2012).
24. W.-Y. Li and S.-H. Chen, "Simulation of normal anchoring nematic droplets under electrical fields," Jpn. J. Appl. Phys. **38**, 1482–1487 (1999).
25. J. H. Erdmann, S. Žumer, and J. W. Doane, "Configuration transition in a nematic liquid crystal confined to a small spherical cavity," Phys. Rev. Lett. **64**(16), 1907–1910 (1990).
26. V. G. Bondar, O. D. Lavrentovich, and V. M. Pergamenshchik, "Threshold of structural hedgehog-ring transition in drops of a nematic in an alternating electric field," Zh. Eksp. Teor. Fiz. **101**, 111–125 (1992).

1. Introduction

Nematic liquid crystals (NLCs) are orientationally ordered liquids of elongated organic molecules, which are spontaneously aligned along a direction, called the director [1]. Their optical, dielectric, magnetic and viscoelastic properties are anisotropic [1]. Because they are optically birefringent elastic fluids, the NLCs exhibit a large optical response under external electric or magnetic fields, which is exploited in all liquid crystal display devices. In these devices the NLCs are confined between two parallel glass plates, which are pre-treated to remove structural defects in the sample. The NLCs are characterized by point or loop topological defects, which appear due to the spontaneous breaking of the isotropic symmetry, confinement, or colloidal inclusions. Thus defects in liquid crystals are undesirable in any practical application of liquid crystals although they are very important and interesting from the standpoint of fundamental physics. Apart from their spontaneous creation during a phase transition, these defects can also be harvested and manipulated in a controlled manner by dispersing foreign micro particles in the liquid crystals [2–7].

In the last two decades various interesting aspects of these defects starting from topology to photonics have been studied extensively [8]. It has been shown that dispersed colloidal microparticles can induce topological defects and interact via long-range forces. Several interesting two and three-dimensional colloidal structures have been reported opening the possibility of tunable photonic colloidal crystals. Recently an interesting new material has been discovered, where the topological defects are crucial for the onset and stabilization of ferromagnetism in a nematic liquid crystal [9]. In such a material, nanometer-size ferrimagnetic platelets are dispersed in the nematic liquid crystal and the dispersion is stabilized by the balance between the magnetic and colloidal forces due to topological defects accompanying these solid ferrimagnetic platelets. Ferromagnetic nematic liquid crystal exhibits stable domains with ferromagnetic dipole moment, which respond linearly and reorient under very weak magnetic field [10, 11]. This discovery created immense interest in the liquid crystal community and subsequently several interesting aspects of these materials were reported [12, 13]. In most of these studies the

Optics EXPRESS

LCs were confined in between two parallel glass plates, whereas dispersions of ferromagnetic nematic LC in immiscible carrier fluid has remained unexplored. In this work we investigate the optical properties of tens-of-micrometer diameter droplets of a ferromagnetic nematic LC in glycerol/lecithin mixture. The confinement of liquid crystals in spherical micro-volume spontaneously creates topological defects depending on their surface anchoring and elasticity. External electric and magnetic fields can deform the director field inside the droplets and modify the defects. This consequently changes optical properties of droplets. Such microdroplets are very interesting for various applications, such as tunable Whispering Gallery Mode (WGM) micro-resonators, 3D-chiral nematic microlasers and WGM nematic microlasers for detecting surfactants or biomolecules [14–21].

External magnetic field has been shown to tune WGM resonances in a photonic crystal fiber filled with a magnetic fluid [22]. In this paper however we investigate the effect of external magnetic field on the spectrum of WGM lasing from ferromagnetic nematic microdroplets immersed in a glycerol-lecithin matrix. We show that the ferromagnetic nematic retains a radial structure with a topological defect in the center of the droplet. External magnetic field couples linearly to the spontaneous magnetization of the ferromagnetic nematic and induces elastic distortion. The distortion mostly starts from the center of the droplet, gradually propagates towards the interface and changes the lasing wavelength of WGM resonances. The observed wavelength shifts are linear in the applied magnetic field.

2. Experimental

For the experiment we used E7, a room temperature nematic liquid crystal (Merck). It exhibits a phase transition to isotropic phase at 58°C. We prepared a suspension of scandium-doped barium hexaferrite single-crystal (Sc-doped $BaFe_{12}O_{19}$) magnetic nanoplatelets in isopropanol, as described previously [9]. The thickness of the platelets is about 5nm, the platelet diameter is distributed around 70 nm with the standard deviation of 38 nm. Further details of the synthesis of the magnetic nanoplatelets and basic characterization can be found in [23]. The suspension was added into the E7 in appropriate quantities and following the reported procedures the ferromagnetic nematic samples were prepared.

We added and thoroughly mixed a small percentage of fluorescent dye, which was either DCM or Nile red, with the ferromagnetic nematic sample. We observed that the magnetic field response was drastically reduced when DCM was added. This suggests that the homeotropic anchoring of LC molecules on the magnetic nanoplatelets, which is crucial for the stabilization of dispersion, is affected by the DCM dye. As a result, the nanoplatelets aggregate and these aggregates get sedimented. Later we doped the ferromagnetic nematic with Nile red dye and found that for the small-enough concentration of the dye the magnetic response remains unchanged for weeks. Hence in all the experiments we used Nile red as fluorescent dye. Still the concentration of the dye had to be optimized: if it was too small, lasing was not excited in the droplets and if it was too big, the ferrimagnetic nanoparticles would sediment.

To produce small ferromagnetic nematic droplets, a small quantity of the dye-doped sample was taken with a tip of the needle and mixed into glycerol/lecithin mixture. Glycerol does not mix with the E7 and usually provides planar anchoring, hence a small amount of lecithin (2 wt%) was added to provide homeotropic (perpendicular) surface anchoring of the director on the surface of ferromagnetic nematic droplets. The mixing of the dye-doped sample into the mixture of lecithin in glycerol was done manually to form micro-droplets of ferromagnetic nematic liquid crystal. The dispersion was then enclosed in a glass cell of thickness about 40 to 50 μm.

The experiments were performed on an inverted optical polarizing microscope (Nikon Eclipse TE2000-U). The schematic diagram of the setup is given in Fig. 1. The sample was observed and pumped through a 60 X water immersion objective with high numerical aperture

Optics EXPRESS

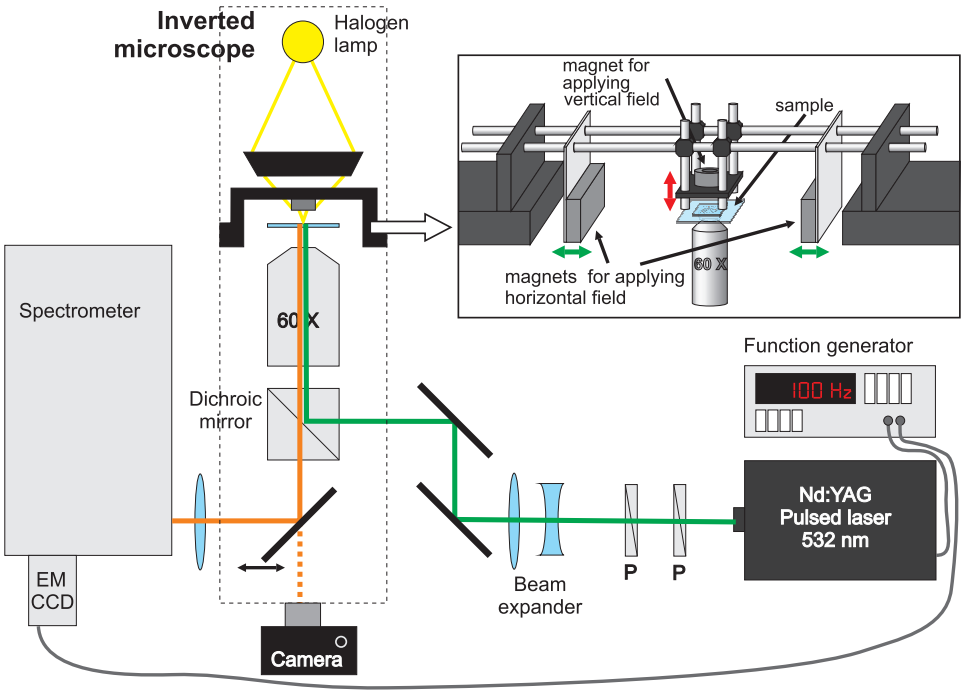

Fig. 1. Schematic diagram of the experimental setup. A Q-switched doubled Nd:YAG laser, triggered by the function generator, is used to induce fluorescence in the droplets, self-assembled from a suspension of ferrimagnetic nanoplatelets (Sc-doped $BaFe_{12}O_{19}$) in E7 liquid crystal and dyed with Nile red fluorescent dye. The spectrum of light emitted from the droplets is detected by the spectrometer, and the images are taken by the camera. Inset shows a setup, mounted on a microscope stage, used for applying the magnetic field either in vertical or in horizontal direction. Green and red arrows denote possible direction of movement of the magnets.

(NA = 1). An actively Q-switched doubled Nd:YAG laser at a wavelength of 532 nm, pulse length 1 ns, maximum repetition rate 10 kHz and maximum pulse energy 10 μJ, was used as the excitation source (Alphalas, Pulselas-A-1064-500). It was triggered with a function generator, the repetition rate was set to 100 Hz. An imaging spectrometer with a 0.05 nm resolution (Andor, Shamrock SR-500i) equipped with a cooled EM-CCD camera (Andor, Newton DU970N) was used to measure the fluorescence and lasing spectra of the droplets, and a CCD camera (Canon EOS 550D) was used to take photomicrographs.

In the inset of Fig. 1 we show the setup for exposing the sample to the magnetic field. We used two flat permanent magnets on rails to apply horizontal magnetic field as homogeneously as possible. By moving the magnets along the rails (movement denoted by green arrows) and varying their distance to the center of the cell, magnetic field at the sample position could be changed from 20 to 100 mT. Vertical magnetic field was applied with another magnet that could be moved along shorter vertical rails (red arrow). In this way the vertical magnetic field could be changed from 10 to 100 mT. This magnet had a shape of a hollow cylinder, so the sample could still be illuminated through the central hole when vertical field was applied. Thus we were able to take photos of the droplets at different vertical field values. Although the magnetic field due to such a magnet is usually not homogeneous it does not change much on a scale comparable to the droplet size (ten micrometers). In experiments we took cross-polarized and lambda plate (red plate) images of droplets in varying magnetic field (horizontal and vertical). Then the droplet

Optics EXPRESS

was positioned so the laser pumped it at the edge and the WGM lasing spectrum was measured while changing the values of the magnetic field.

3. Results and discussion

When ferromagnetic nematic droplets are produced they appear radial and many of them contain visible particles - aggregates of ferrimagnetic nanoplatelets - preferably located in the droplet center. In Fig. 2 we show a series of images with increasing horizontal magnetic field taken under crossed polarizers. The corresponding images taken with a red-plate are also shown. A black arrow marks the direction of the magnetic field $\vec{B}$.

Already at small magnetic field of 20 mT, which is the smallest magnetic field we could apply, we see in crossed-polarizers image in Fig. 2(a) that the director structure is slightly distorted and asymmetric. Four dark brushes between crossed polarizers suggest that the structure of the director is radial. Each of them starts perpendicular at the surface of the droplet and is continued towards the center, where a radial hedgehog defect is formed. Already at a moderate field of 30 mT [Fig. 2(b)], there are two brighter lobes (left one indicated by a white arrow), which are located half-way to the left and right of the center. In the center, a thread-like structure is formed, most likely a collection of magnetic nanoparticles. It looks like a projection of a disk, trapped in the center of the droplet. This thread-like structure is also visible in red-plate images in Figs. 2(e)–2(h). The bright lobes, denoted with white arrows in Figs. 2(b)–(d), become more pronounced at higher magnetic field.

Figure 3 shows a droplet in increasing vertical magnetic field pointing out of the plane between crossed polarizers and corresponding red-plate images. At small magnetic field (20 mT) the droplet appears radial with four straight brushes emerging from its center followed by a series of concentric and colored rings. Already at a small magnetic field of 20 mT, the structure is not rotationally symmetric when viewed under crossed polarizers. This is clearly seen in Fig. 3(a), where the horizontal dark brush is again slightly brighter midway between the center

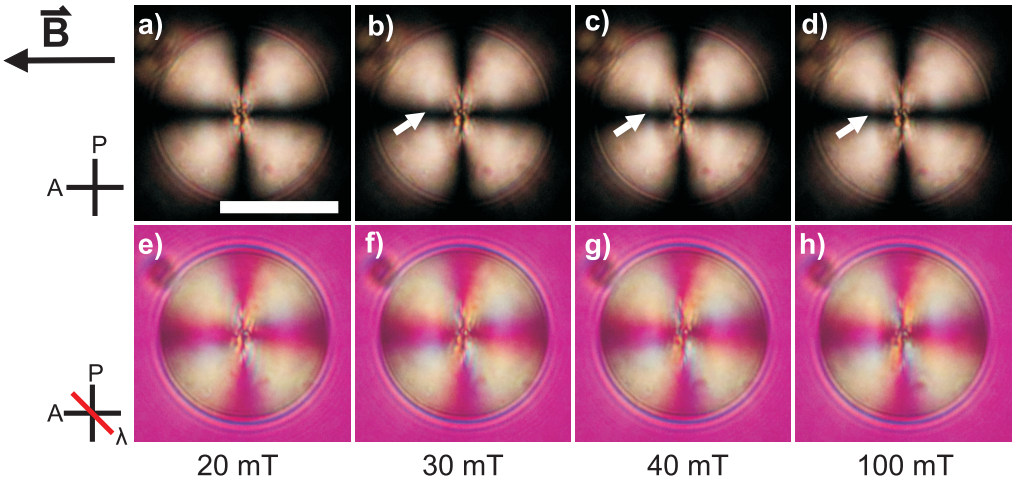

Fig. 2. Ferromagnetic nematic droplet in an increasing horizontal (in-plane of the sample) magnetic field. The black arrow marks the direction of the magnetic field $\vec{B}$. (a)–(d) Distortion inside the droplet as observed under crossed polarizers, when field is increased from 20 mT to 100 mT. White arrows mark the bright lobes that appear when the droplet is exposed to magnetic field. The lobes become more evident when field is increased. (e)–(h) Lambda plate images of the distortion at the same magnetic field values. Lambda plate is inserted at 45°, as indicated in schematics left of (e). Scale bar 20 μm.

Optics EXPRESS

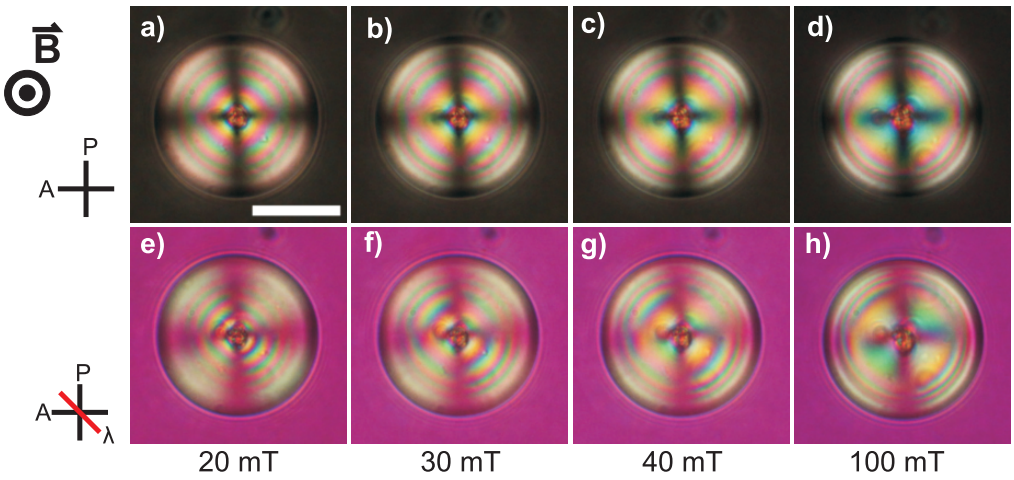

Fig. 3. Ferromagnetic nematic droplet in increasing vertical magnetic field. Direction of the magnetic field is out of the plane. (a)–(d) Distortion inside the droplet imaged under crossed polarizers when field is increased from 20 mT to 100 mT. (e)–(h) Lambda plate images of the distortion at the same magnetic field values. Lambda plate is inserted at 45° as indicated in schematics left of (e). Scale bar 20 μm.

and the surface of the droplet. By increasing magnetic field, the circles are pushed towards the droplet surface and the central part of the droplet gets large areas of uniform color. The discontinuity of the dark brush is here clearly visible at 100 mT in Fig. 3(d). When the magnetic field is increased, these brushes move further towards the droplet edge indicating larger volume of distorted liquid crystal, with molecules pointing along $\vec{B}$. Lambda plate images in Figs. 3(e)–3(h) suggest that in this area the two dimensional projection of the director is pointing in the radial direction. The increasing intensities of yellow and blue in the central area, when observed with lambda-plate, suggest that the molecular tilt is gradually increasing and more and more molecules align into the $\vec{B}$ direction. In comparison with distortions, caused by the electric field [14, 24–26], the observed distortions due to magnetic field seem more complex and harder to figure out and should be analyzed further with numerical simulations.

These optical observations clearly indicate that a nematic director field in a ferromagnetic nematic droplet is strongly influenced by an external magnetic field. The optical changes should therefore influence the spectrum of WGM resonances in droplets, and they should be reflected in the WGM lasing spectra from droplets in an external magnetic field. We therefore explored whether there is any WGM lasing from the dye-doped ferromagnetic nematic droplets. They were illuminated by 1 ns pulses from the 532 nm laser and the spectrum of the emitted light was measured as a function of the excitation energy.

Figures 4(a) and 4(b) show optical micrographs of the emission pattern on the droplet and spectrum of the ferromagnetic nematic droplet below the lasing threshold. The emitted light intensity in this region is smooth across the droplet and has a maximum at the position of WGMs. It is therefore characteristic of an incoherent and narrow band light source. However, the emission pattern is quite different above the threshold, when the droplet gets into the lasing regime, as shown in Fig. 4(c). We observe under a microscope a red speckle pattern, which is characteristic for coherent emitted light. Figure 4(d) shows a corresponding spectrum above the threshold for lasing, showing a set of lines, which are evidently narrower than below the threshold in Fig. 4(b). Figure 4(e) shows a typical 2-slope lasing behavior with a threshold energy around 170 nJ for a 1 ns pumping pulse, focused to a few micron spot on the droplet edge. The inset to Figure 4(e) shows the dependence of the emitted linewidth on the pump energy. There is a clear

Optics EXPRESS

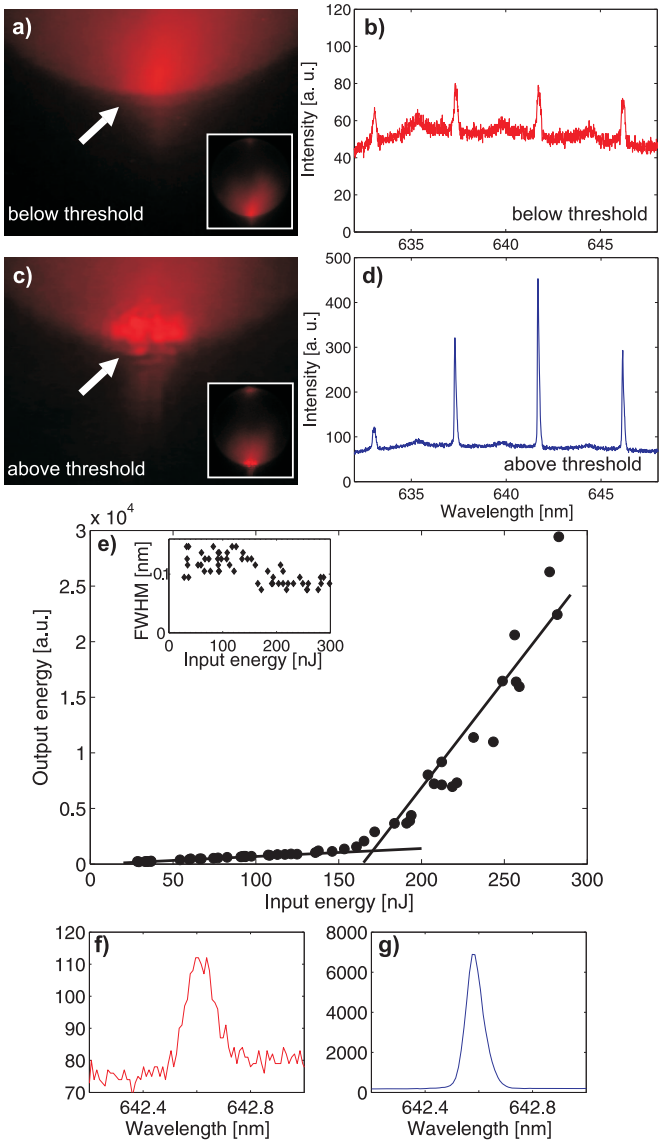

Fig. 4. WGM lasing from a typical Nile red-doped ferromagnetic nematic droplet. (a) Microscope image of emission pattern at the droplet edge below the threshold for lasing. The inset shows emission pattern for the whole droplet, when it is pumped at the bottom edge. (b) Typical WGM spectrum below the lasing threshold. (c) Microscope image of emission pattern at the droplet edge in the lasing regime. Red speckle pattern (marked with a white arrow) is seen, which is characteristic for coherent emitted light. Emission pattern for the whole droplet is shown in the inset. (d) Typical WGM spectrum above the lasing threshold. If compared to the spectrum in (a), linewidth reduction can be observed above the lasing threshold. (e) Intensity of a WGM peak as a function of the input-pulse energy density. A typical 2-slope lasing curve is observed. The lines are added as guides for the eye, indicating lasing threshold at ~170 nJ. The inset shows the linewidth dependency on input energy showing reduction at the onset of lasing. (f) WGM line below the threshold. (g) Above the threshold the width of the WGM line is reduced.

Optics EXPRESS

reduction of the linewidth of the emitted light above the lasing threshold, which is characteristics of lasing. Figures 4(f) and 4(g) show a typical WGM line below and above the threshold, respectively. The threshold energy is larger than the typical threshold value of common nematic liquid crystal droplets. This is due to high absorption of light in the ferrimagnetic nanoparticles and the low dye concentration that is needed to prevent sedimentation of the nanoplatelets.

We then studied the effect of magnetic field on the lasing in external magnetic field, applied in two different directions with respect to the plane of circulation of WGMs. In the first configuration the magnetic field is in-plane of WGM circulation, in the second configuration it is out-of plane. The pump laser intensity had to be optimized for each droplet: the intensity had to be high enough for the droplet to be in the lasing regime, but not too high, as that caused burning of the droplet due to high absorption of light by the ferrimagnetic nanoplatelets.

The WGM lasing in the in-plane configuration is shown in Fig. 5. For this configuration, there are three possible experimental configurations of field direction and position of the pump laser spot, which could be realized under the microscope. In all three cases the magnetic field is in plane with the WGM propagation, but the direction of the magnetic field is either in-plane of the sample, as in Fig. 5(a), or perpendicular to the plane of the sample, as in Figs. 5(b) and 5(c). In all cases, the WGM wavelength shifts to the blue part of the spectrum with increasing magnetic field, as shown in Fig. 5(d). The shift is linear in the field and fully reversible, as can be seen from both panels in Fig. 5(d). The blue-shift for the in-plane configuration is $\approx$ 1 nm for the highest applied field of 100 mT, and depends on the droplet size and condition.

In our experimental setting, there is only one way to realize WGM lasing in the out-of-plane configuration, which is shown in Fig. 6. Here the magnetic field is in the plane of the sample and the plane of WGM circulation is perpendicular to it, as shown in Fig. 6(a). The corresponding spectrum shifts to the red part of the spectrum when the magnetic field is applied, as shown in Fig. 6(b). This red-shift is opposite to the blue-shift, which was observed for the three in-plane

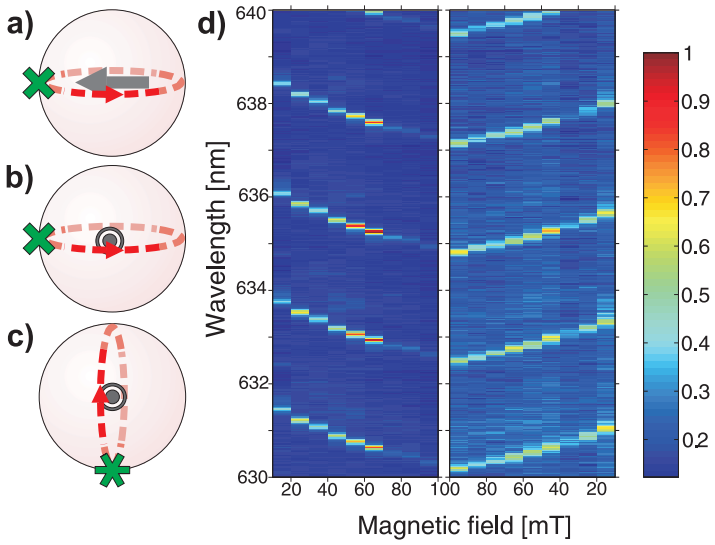

Fig. 5. Wavelength shift of WGM lasing in external magnetic field for the in-plane configurations. (a)–(c) Three possible experimental configurations of $\vec{B}$ direction and pump laser spot position. In these configurations the magnetic field $\vec{B}$ is in-plane with WGM circulation. (d) Magnetic-field dependence of the WGM lasing spectrum. The lasing lines shift towards the blue part of the spectrum, the shift is linear in the magnetic field and fully reversible. The magnetic lineshift is of the order of 1 nm/100 mT.

Optics EXPRESS

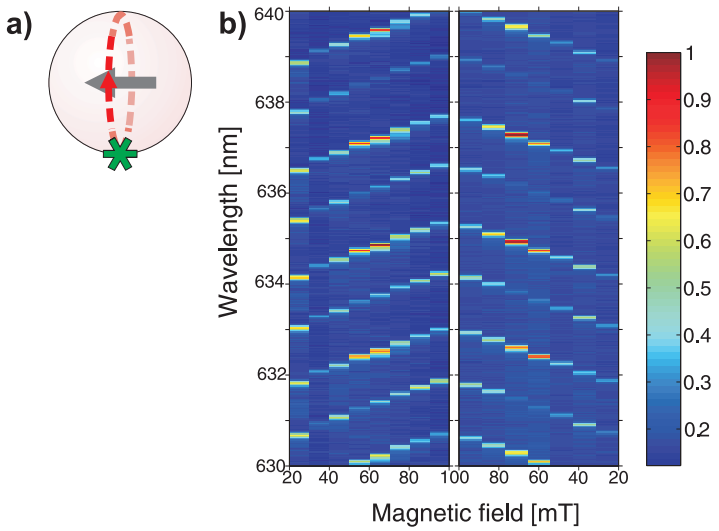

Fig. 6. Wavelength shift of WGM lasing in external magnetic field for the out-of-plane configuration. (a) Configuration of field direction and pump laser location in the experiments. (b) Magnetic field shifting on the lasing spectrum in the out-of-plane configuration towards the red part of the spectrum. The red-shift is ≈ 1 nm/ 100 mT.

configurations in Fig. 5. The red-shift is again linear in magnetic field and its magnitude is slightly higher than 1 nm/ 100 mT. The shift is again fully reversible, as can be seen from two panels in Fig. 6(b).

In zero magnetic field the birefringence is ≈ 4% lower than in the pure E7, most likely because the nano-particles cause disorder in the director field due to their shape. However, in nonzero magnetic field the fluctuations are reduced and therefore the birefringence increases. When the magnetic field is applied, the birefringence is increased and we estimate upper boundary for the birefringence increase to about 3×10^{-6}/mT. The birefringence does not change linearly with the magnetic field, rather it starts to saturate. When magnetic field is increased from 0 to 100 mT, the maximum wavelength shift that can be attributed to the birefringence increase, is small - within the width of the WGM peak. The majority of the wavelength shift is therefore due to distortions caused by the magnetic field.

The maximal shift that was observed in any experiment was when the peaks shifted towards red for 2 nm. The extent to which the peak wavelengths move, depends on various parameters including the time the sample has been mixed with Nile Red, the number of aggregates in the droplet, how well the pump laser position coincides with the droplet edge, etc. In any case the shifts of the lasing spectra in external magnetic field are not very large in comparison to the effect of external electric field, where the reported shift was about 10 nm at 1 V/μm [14]. However, in contrast to quadratic field dependence in the case of AC external electric field, the lasing spectrum in the case of ferromagnetic nematic droplets shifts linearly with the magnetic field. This linearity is a great advantage in possible applications of this magneto-optic effect, as the effect is evident already at small magnetic fields.

The main reason for rather small sensitivity to external magnetic fields is that the director at the boundary remains almost unchanged due to the strong surface anchoring. The distortion is taking place mostly in the bulk, which is also visible in polarizing micrographs, whereas the WGM modes are localized close to the surface of the droplet. A larger shift may be expected in the case of weak surface anchoring with the distortion taking place near the boundary. Further progress in this direction is underway and will be reported elsewhere.

Optics EXPRESS

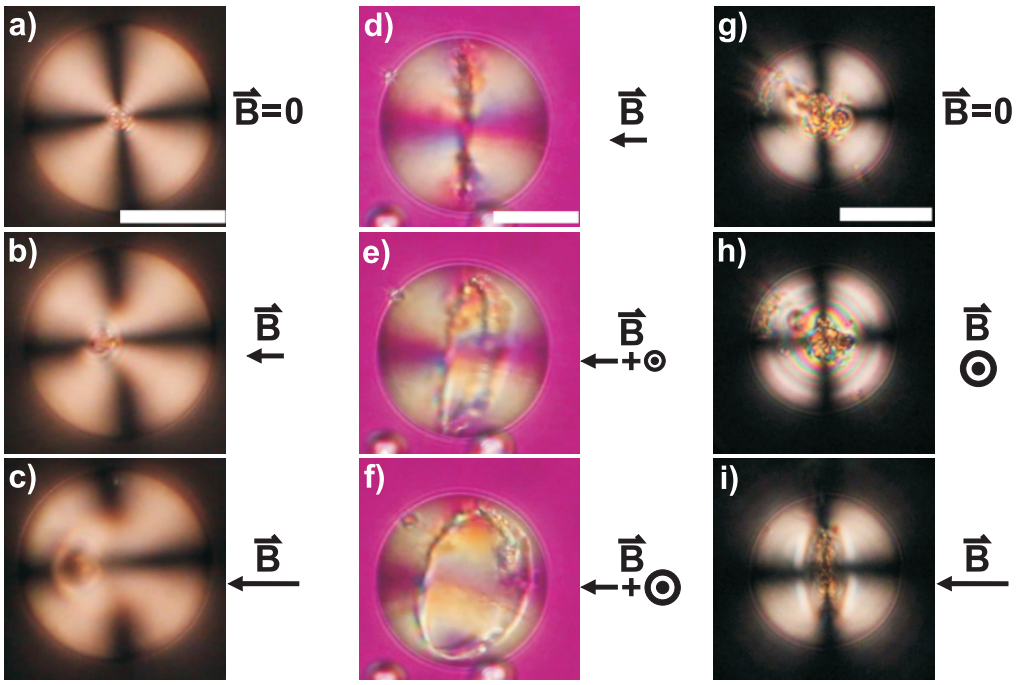

Fig. 7. Interesting behavior of some ferromagnetic nematic droplets in magnetic field. (a)–(c) The center of the droplet, containing an aggregate of nanoplatelets, moves along the direction of the applied magnetic field. (d)–(e) This droplet contains agglomerated nanoplatelets arranged in a ring close to the droplet surface. In (d) the droplet is in horizontal field. In (e) a perpendicular field component of magnetic field is added, making the overall field direction turn and the ring structure visible. In (f) the vertical component of the magnetic field is increased, making the ring turn further. (g)–(i) A droplet with a large aggregate in the center is shown first (in (g)) in zero magnetic field, in (h) we can see it in vertical field and in (i) in horizontal field. In this case the aggregated nanoplatelets form a disc-like shape, turning perpendicularly to magnetic field direction.

Finally we show in Fig. 7 some interesting cases of droplet structure and response in magnetic field, that could enlighten the nature of elastic distortions and director structures in different droplets. Figures 7(a)–7(c) show crossed-polarizer images of a droplet with an aggregate of nanoplatelets in the center. When magnetic field is applied, the aggregate moves along the field direction. In this case the magnetic field was applied using a single magnet and its direction was slightly out of plane at high values, that is why in Fig. 7(c) the aggregate is also moved out of plane as it follows the magnetic field direction. The second case [Figs. 7(d)–7(f)] shows lambda-plate images of the droplet that contains agglomerated nanoplatelets, arranged in a ring close to the surface of the droplet. The field is horizontal in Fig. 7(d) and then a perpendicular component is added, resulting in a rotation of the ring, as shown in Figs. 7(e) and 7(f). The magnetic dipoles in the droplet tend to align with the magnetic field and the ring structure becomes visible. The ring positions itself perpendicularly to the magnetic field direction $\vec{B}$. Figures 7(g)–7(i) show another droplet with a large aggregate in the center under crossed polarizers. There is no distortion in zero magnetic field [Fig. 7(g)], but as the droplet has previously been exposed to a vertical magnetic field, the aggregate is positioned same as in the case when the field is vertical [Fig. 7(h)]. However, in vertical field we can see that distortions appear throughout the droplet. In Fig. 7(i) the droplet is shown in horizontal field. We can see that the aggregated nanoplatelets in this droplet form a disc, which orients perpendicularly to the magnetic field.

Optics EXPRESS

4. Conclusion

We present first studies of WGM lasing from ferromagnetic nematic droplets with perpendicular surface anchoring in an external magnetic field. In most of the droplets studied, the director is distorted by the magnetic field and is keeping the radial configuration. The WGM lasing exhibits a wavelength shift that is in all cases linear with the external field. However, the direction of the shift depends on the geometry of the lasing experiments. When the external magnetic field is in-plane of the WGM circulation, the modes shift linearly towards the blue part of the spectrum. When the magnetic field is perpendicular to the plane of circulation of WGMs, the shift is towards the red end of the spectrum. In both cases we measure similar magnitude of the shift, which is ≈ 1 nm/ 100 mT. The shifts are fully reversible and stable. We estimate that the sensitivity of ferromagnetic nematic droplets is limited to the linewidth of the emitted laser light, which is around 0.1 nm. Therefore the magnetic fields of the order of 10 mT could be detected by measuring the magnetic field induced shifts of the WGM lasing lines. The linearity of the magnetic-field-induced shift is understood because of the linear coupling of the magnetic field $\vec{B}$ to the local density of magnetization $\vec{M}$ in ferromagnetic nematic droplets. On the other hand, it is difficult to explain opposite directions of the shifts for two different configurations. This indicates that the magnetic field induced distortion of ferromagnetic nematic droplets is not quite trivial and has to be analyzed within numerical simulations of the director-magnetization coupled fields of a droplet in an external magnetic field.

Funding

Slovenian Research Agency (ARRS) (PR-05543, P1-0099, J1-6723, P1-0192, P2-0084); SERB (EMR/2015/001566); UPE-II; DST/SJF/PSA-02/2014-15; DST-PURSE; J. A. S. acknowledges UGC-BSR for fellowship.